Available online at www.sciencedirect.com
ScienceDirect
Journal of Solid State Chemistry 180 (2007) 1713–1719
JOURNAL OF SOLID STATE CHEMISTRY
www.elsevier.com/locate/jssc

Building up 3-D framework structure from interlinking layered cobalt phosphates and organic pillars

Wei-Kuo Chang[a,b], Ray-Kuang Chiang[b,*], Sue-Lein Wang[a,**]

[a]*Department of Chemistry, National Tsing Hua University, Hsinchu 30013, Taiwan, ROC*
[b]*Department of Electronic Materials, Far East University, Tainan 74448, Taiwan, ROC*

Received 12 December 2006; received in revised form 2 March 2007; accepted 11 March 2007
Available online 21 March 2007

Abstract

A new cobalt phosphates (trans-1,4-dach)$_{0.5}$Co$_3$(H$_2$O)(OH)(PO$_4$)(HPO$_4$)$\cdot(3+x)$H$_2$O (**1**), has been synthesized under a hydrothermal condition and structurally characterized by single-crystal X-ray diffraction. It consists of cobalt phosphates layers and coordinated bis-N-donor ligands, trans-1,4-diaminocyclohexane, which are interlinked to form a 3-D framework structure with 1-D tunnel occupied by water molecules. When its channel water is fully removed at a relatively low temperature, the pillars fold up, and no porosity can be detected by sorption. However, the structural integrity of the compound is retained, and the pillar can still rise to its original upright position after contact with water vapor. This implies that some channel water molecules play a wedge function to control the up and down positions of the organic bis-N-donor ligands. When **1** is partially dehydrated, it revealed adsorption of various linear organic molecules, although the fully dehydrated one did not adsorb any organic molecules. Magnetic susceptibility measurements showed that **1** is an antiferromagnet with a canted interaction at a transition temperature of about 10 K. Crystal data: monoclinic, $C2/c$, $a = 28.653(10)$ Å, $b = 12.874(4)$ Å, $c = 8.266(3)$ Å, $\beta = 97.257(7)$, $V = 3025(2)$ Å3, $Z = 8$.

Keywords: Cobalt phosphates; Organic pillars; Crystal structures

1. Introduction

Layered organic–inorganic hybrid materials have received a lot of research interest because of their combined organic–inorganic feature which has tailored applications in catalysis, adsorption, and separation [1–4]. Most of the layered organic–inorganic hybrid materials have a structural moiety of inorganic layer and pendent organic groups pointing toward the interlayered space [5–7]. The expandability between the interlayered spaces provides a good place for studying guest–host interaction between the inserted organic molecules and the organic groups attached on the inorganic layers [8–15]. Frequently, this type of structure is synthesized from building units of organo phosphonate ligands (or diphosphonate ligands) and metal salts. A similar strategy following this line is to prepare microporous materials by interlinking layered inorganic moieties with bidentate N-donor ligands. For example, several 4,4′-bipyridine pillared V [16–19], In [20], Ga [21,22], Cu [16], and Co [23], phosphates have been reported recently. Transition metal phosphate sheets are interlinked covalently by rigid 4,4′-bipyridine ligands via self-assembling process resulting in microporosity. Typically, they were obtained in a mixture of bifunction amine, metal salts, and phosphoric acid by hydrothermal reactions. The bifunctional amines not only act as N-donor ligand to complete the metal coordination sphere but also function as spacers between the adjacent inorganic metal phosphates layers. For an easily formed layered metal phosphate with accessible coordination sites and flexible charge-balancing capabilities, one may envisage the possibility of synthesizing analogous 3-D structures containing the same inorganic layers but pillared with different bidentate organic molecules. For example, we reported recently that [Co$_3$(pyr)(HPO$_4$)$_2$F$_2$] and [Co$_3$(4,4′-bpy)

*Corresponding author. Fax: +886 6 597 7767.
**Also corresponding author.
E-mail addresses: rkc.chem@msa.hinet.net (R.-K. Chiang), slwang@chem.nthu.edu.tw (S.-L. Wang).

0022-4596/$ - see front matter © 2007 Elsevier Inc. All rights reserved.
doi:10.1016/j.jssc.2007.03.015

$(HPO_4)_2F_2 \cdot xH_2O$] [23] contain the same neutral sheets of fluorinated cobalt phosphate but pillared through pyrazine and 4,4′-bipyridine molecules, respectively. In this paper, we found another layered cobalt phosphate, $Co_2(OH)_2(H_3O)(HPO_4)(H_2PO_4)$ (**2**) [24], which can be easily formed in a broad range of pH values from 3 to 10 in the $CoO–P_2O_5–H_2O$ system, and can function as an inorganic part in the process of formation of organic–inorganic hybrid structures. Based on this layered structure, related 3-D framework phosphates which are pillared through trans-1,4-diaminocyclohexane ligands was synthesized. Here we report its synthesis, structure chemistry, and adsorption properties.

2. Experimental section

2.1. Synthesis

A mixture of $CoCl_2 \cdot 6H_2O$ (1.0 mmol), H_3PO_3 (2.0 mmol), trans-1,4-diaminocyclohexane (2.7 mmol), and H_2O (10 mL) was stirred overnight in a Teflon cup. It was then sealed in an acid digestion bomb and heated to 160 °C for 72 h followed by slow cooling (6 °C/h) to room temperature. The product was recovered by filtering off and gave plate-like blue crystals of **1** mixed with some unidentified pink powder. Crystals of **1** suitable for single-crystal X-ray analysis were selected, and the structural determination indicated it as a new phase. **1** in a pure form can be obtained by heating a mixture of $CoCl_2 \cdot 6H_2O$ (1.5 mmol), H_3PO_4 (1.0 mmol), trans-1,4-diaminocyclohexane (2.9 mmol), and H_2O (10 mL) under the same reaction conditions as above. The initial and final pH of the reaction solution was unchanged (10.2). The resulting mixture was recovered by filtering off and gave fine blue powder as product. The XRD pattern of the blue powder is consistent well with the pattern simulated from the coordinates of the previous blue crystals. Electron probe microanalysis confirmed the Co to P ratio of 3 to 2. The elemental analysis of the blue powder was also consistent with the formula from single-crystal study (Anal. found/Calcd.: C, 6.78/6.79; H, 3.32/3.42; N, 2.49/2.64). Based on the combined evidence, the blue powder was used as the pure form of **1** for further physical analyses.

2.2. Single-crystal structure analyses

Before a satisfactory crystal was obtained, many selected crystals of **1** were twinned based on the reflection profiles. Eventually, a blue crystal of dimensions $0.10 \times 0.10 \times 0.02\,mm^3$ was selected for indexing and intensity data was collected on a Siemens SMART CCD diffractometer equipped with normal focus, 3-kW sealed tube X-ray source. Intensity data were collected at room temperature in 1271 frames with ω scans (width 0.30° per frame) and corrected for Lp and adsorption effects using the SADABS program [25]. Number of measured and unique reflections with $I > 2\sigma I$ are 11 099 and 3755. On the basis of reflection conditions, statistical analysis of the intensity distributions, and successful solution and refinement of the structure, the space group was determined to be $C2/c$ (no. 15). Direct methods were used to locate the Co atoms and P atoms first, and the remaining oxygen, carbon, and nitrogen atom were found from successive difference maps. There were seven bridged oxygens shared by Co and P atoms with values of bond-valence summations (BVS) [26] from 1.74 to 2.02. The BVS of unbridged oxygen O4 has a low value 1.32, indicating that O4 was hydroxyl group. BVS of O9 and O10 were even lower (0.51 and 0.62). The H atoms of trans-1,4-diaminocyclohexane were located in difference Fourier maps. The final cycles of least-squares refinement including atomic coordinates and anisotropic thermal parameters for all non-hydrogen atoms converged at $R1 = 0.0590$ and $wR2 = 0.1369$. All calculations were performed using SHELXTL Version 5.1 software package [27]. The crystallographic data were summarized in Table 1.

2.3. Temperature dependent X-ray powder diffraction

XRD patterns of the sample were recorded on a SHIMADZU XRD-6000 X-ray diffractometer with a HTK 1200 high temperature oven camera (Anton Paar) using Cu$K\alpha$ radiation with a voltage of 40 kV and of 30 mA. Variable-temperature in situ XRD experiment was carried out from room temperature to 800 °C at a rate of 10 °C/min. For each pattern the step-scan rate is 2° (2θ/min).

2.4. Thermogravimetric and sorption analyses

Thermogravimetric measurement (TGA7 Perkin-Elmer Instruments) was carried out in dried nitrogen at a heating rate of 10 °C/min with sample of about 10 mg. In the

Table 1
Crystallographic data for compound **1**

Formula	$C_3H_{16}Co_3NO_{13}P_2$
fw	512.90
Space group	$C2/c$
a (Å)	28.653(1)
b (Å)	12.874(4)
c (Å)	8.266(3)
β (deg)	97.257(7)
V (Å^3)	3025(2)
Z	8
No. refltn collected	10828 ($3755 > 2\sigma(I)$)
T (K)	295(2)
λ (Å)	0.71073
ρ calcd (g/cm^3)	2.252
μ (mm^{-1})	3.527
$R1$[a]	0.0590
w$R2$[b]	0.1369

[a] $R1 = \sum||F_o|—|F_c||/\sum|F_o|$.
[b] $wR2 = [\sum w(|F_o|^2—|F_c|^2)^2]/\sum w(|F_o|^2)^2]^{1/2}$, $w = [\sigma^2(F_o^2) + 0.0752P]^2$, where $P = (F_o^2 + 2F_c^2)/3$.

sorption experiment, the sample of **1** was first heated to 120 °C (10 °C/min) to partially remove the tunnel water in a flow of dried nitrogen, and then the sample was cooled to room temperature (10 °C/min). At the same time the gas stream was switched from a dried nitrogen to a gas stream of dried nitrogen bubbled through a gas scrubber filled with the adsorbate solvents. The flow rate was 30 cm^3/min based on a mass flowmeter (MKS).

2.5. Magnetic measurements

The magnetic properties were investigated with a commercial SQUID magnetometer in the range of 2–300 K with field of 5000 Oe.

3. Results and discussion

3.1. Structure

The atomic coordinates and thermal parameters were in Table 2, and selected bond lengths and bond valence sums were listed in Table 3. The ORTEP drawing was shown in Fig. 1. There are three unique cobalt atoms and two unique phosphorus atoms in **1**. Both Co1 and Co2 are octahedrally coordinated by six oxygen atoms, while Co3 is tetrahedrally coordinated by three oxygen atoms and one nitrogen atom. P1 and P2 were phosphate groups. The structure of **1** involves ligand-interlinked cobalt phosphate layers through the bis-N-donor ligands of trans-1,4-diaminocyclohexane. Part of the cobalt phosphate layer in **1** is a copy of the known compound $(H_3O)Co_2(OH)_2(HPO_4)(H_2PO_4)$ (**2**). The cobalt phosphate layer consists of zigzag chains of edge shared CoO_6 octahedra, which were fused by corners to form a sheet, and it was also bridged by phosphate groups distributed on both sides of the CoO_6 sheets to form a tri-decked cobalt phosphate layer, Fig. 2. The major difference between compound **1** and **2** is that extra cobalt atoms (Co3) were present as the coordination sites for bridging N-donor ligands between layers in **1**, Fig. 2a. The phosphate group of P1 shares its three corners through one μ-3 oxygen atom (O1), and two μ-2 oxygen atoms (O2 and O3) with octahedral and tetrahedral cobalt, and leaves the fourth one (O4) as a pendant oxygen, Fig. 2a. The BVS calculation of O4 reveals a low value of 1.32 indicating that O4 is a hydroxyl group. The phosphate group of P2 shares its four corners, two μ-3 oxygen atoms (O5 and O6) and two μ-2 oxygen atoms (O7 and O8), which are located between two neighboring cobalt octahedral chains and on the cobalt tetrahedral. The tetrahedral Co3 shares its three corners with the cobalt phosphate layers and the fourth corner is the amine nitrogen of trans-1,4-diaminocyclohexane ligand, Fig. 2a. The values of BVS

Table 2
Atomic coordinates ($\times 10^4$) and thermal parameters ($Å^2 \times 10^3$) for **1**

	x	*y*	*z*	*U*(eq)
Co(1)	2526(1)	6354(1)	666(1)	17(1)
Co(2)	2541(1)	6349(1)	4564(1)	18(1)
Co(3)	3639(1)	3822(1)	6438(2)	30(1)
P(1)	3149(1)	1956(2)	7762(2)	17(1)
P(2)	3137(1)	5400(2)	7948(3)	17(1)
O(1)	2897(2)	7756(4)	4217(6)	19(1)
O(2)	2834(2)	7798(4)	1176(6)	18(1)
O(3)	3592(2)	2605(4)	7795(7)	29(2)
O(4)	3274(2)	814(4)	7813(7)	21(1)
O(5)	3120(2)	5886(4)	−365(7)	19(1)
O(6)	2836(2)	5588(4)	2783(6)	19(1)
O(7)	2969(2)	6187(4)	6670(7)	24(1)
O(8)	3644(2)	5102(4)	7764(8)	30(2)
O(9)	2049(2)	6813(4)	2375(6)	20(1)
O(10)	2133(2)	5021(4)	−84(6)	19(1)
N(1)	4185(3)	3568(7)	5172(10)	49(2)
C(1)	4667(4)	3563(8)	6036(13)	47(3)
C(2)	4754(4)	2579(8)	7050(14)	46(3)
C(3)	4751(4)	4540(8)	7088(16)	55(3)
OW1	4041(3)	3239(7)	10808(9)	64(2)
OW2	1125(4)	6556(12)	1946(15)	135(5)
OW3	814(8)	4730(14)	1720(40)	316(15)

Table 3
Selected bond lengths (Å) and bond valence sums for **1**

Co(1)–O(2)$^{\#1}$	2.044(5)	P(1)−O(3)	1.518(7)
Co(1)–O(2)	2.078(5)	P(1)−O(4)	1.513(5)
Co(1)–O(5)	2.087(6)	P(1)−O(1)$^{\#3}$	1.524(6)
Co(1)–O(6)	2.105(5)	P(1)−O(2)$^{\#3}$	1.527(5)
Co(1)–O(10)	2.102(5)		
Co(1)–O(9)	2.169(6)	P(2)−O(7)	1.499(5)
		P(2)−O(8)	1.526(7)
Co(2)–O(7)	2.011(5)	P(2)−O(6)$^{\#3}$	1.533(6)
Co(2)–O(6)	2.039(5)	P(2)−O(5)$^{\#4}$	1.535(6)
Co(2)–O(1)$^{\#2}$	2.057(5)		
Co(2)–O(1)	2.116(5)		
Co(2)–O(10)$^{\#3}$	2.155(5)	N(1)−C(1)	1.471(12)
Co(2)–O(9)	2.230(5)	C(1)−C(3)	1.530(15)
		C(1)−C(2)	1.523(13)
Co(3)–O(3)	1.942(6)	C(2)−C(2)$^{\#5}$	1.51(2)
Co(3)–O(8)	1.978(6)	C(3)−C(3)$^{\#5}$	1.50(2)
Co(3)–O(5)$^{\#3}$	2.004(5)		
Co(3)–N(1)	2.016(9)		

Symmetry transformations used to generate equivalent atoms: $^{\#1}-x+1/2, -y+3/2, -z$; $^{\#2}-x+1/2, -y+3/2, -z+1$; $^{\#3}x, -y+1, z+1/2$; $^{\#4}x, y, z+1$; $^{\#5}-x+1, y, -z+3/2$.

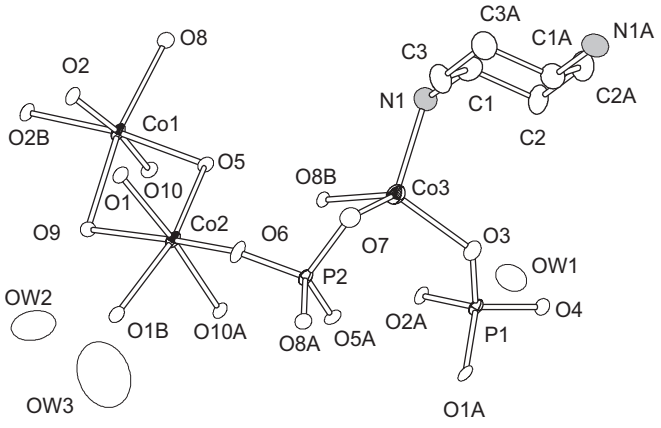

Fig. 1. Building units of **1** showing the atom labeling scheme.

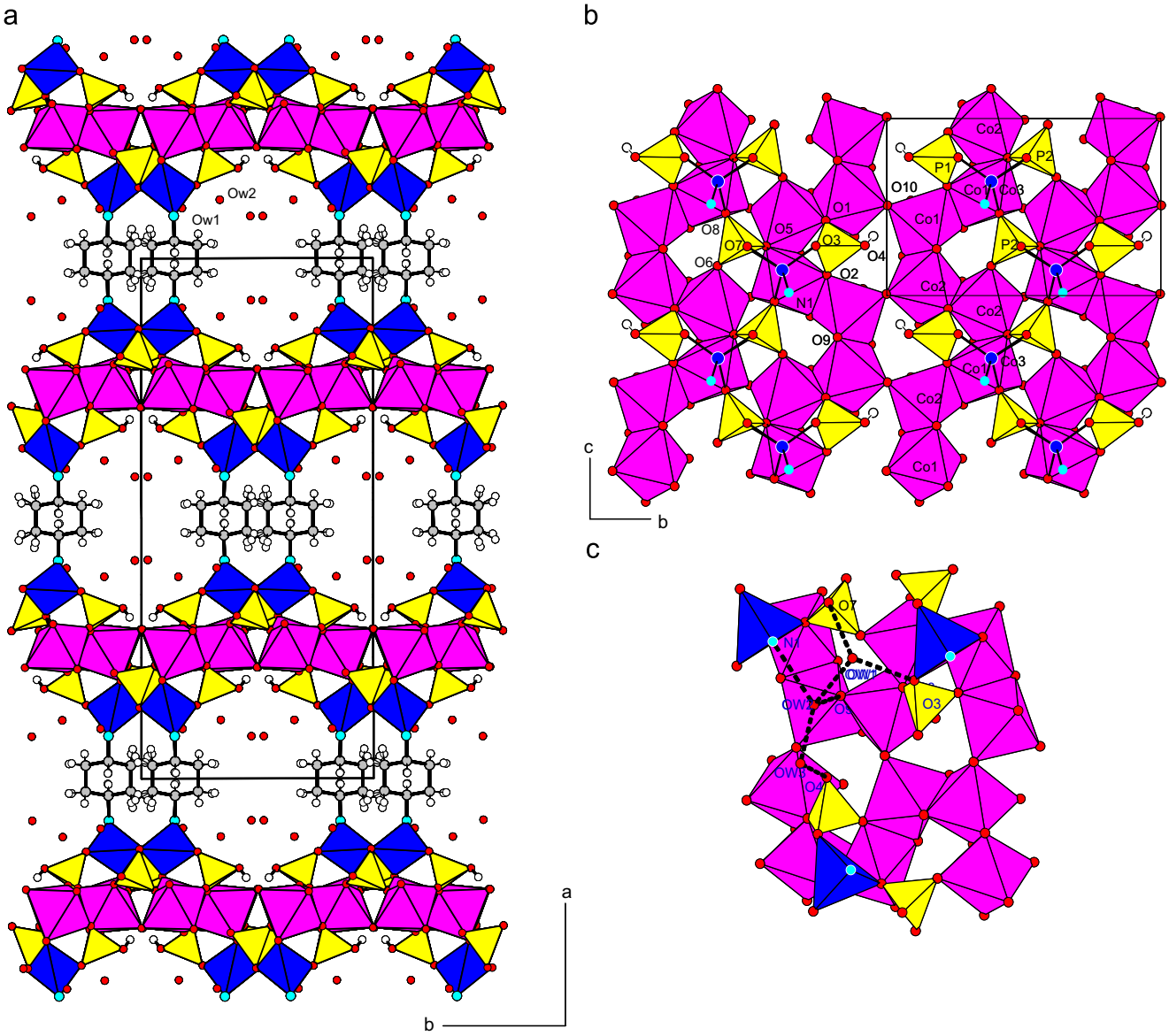

Fig. 2. (a) Structure of **1** viewed along the *c*-axis (the red, blue, and yellow polyhedra represent the cobalt octahedral, cobalt tetrahedral, and phosphate tetrahedral). (b) Structure unit of **1** showing the inorganic layer, phosphate groups on the opposite side are omitted for clarity. (c) Hydrogen bonds between cobalt phosphate layer and channel water molecules. (key: black circle, C atoms; red circle, O atoms; blue circle, N atoms).

calculation of O9 and O10 were quite low (0.51 and 0.62). O9 was located on the edges of the edge-fused CoO_6 chains. O10 was the bridging oxygen atoms between two neighboring edge-fused CoO_6 chains. To assign the correct composition of compound **1**, we need to refer to the above-mentioned compound **2** in Ref. [24]. The formula of **2**, $(H_3O)[Co_2(OH)_2(HPO_4)(H_2PO_4)]$, adapts two more hydrogens on the phosphate groups than that in the formula of **1**, $(\text{trans-1,4-dach})_{0.5}[Co_3(H_2O)(OH)(HPO_4)(PO_4)]\cdot(3+x)H_2O$. Also, in **2**, H_3O instead of water was assigned in the interlayered space by considering the charge compensation when O9 and O10 are both assigned as OH groups. The two positive charges of protons on phosphates in **2** are replaced by the divalent cobalt Co3 in **1**. However, if the O9 and O10 in our compound were both assigned as hydroxyl groups, the interlinking ligand has to be protonated. In viewing that the Co–N distance that is comparable to a common Co–N bond length from our previous studies, we think there should not be enough space for protonation around the nitrogen of the ligand. Both O9 and O10 involve rather strong hydrogen bonds ($d(O4\cdots O10) = 2.57$ Å, $d(Ow2\cdots O9) = 2.65$ Å. Since the hydrogen bonding of O10 appears stronger, O10 could be assigned as a hydroxyl group and O(9) a water molecule. OW1, OW2 and OW3 were three water molecules located in the 1-D tunnels (Fig. 2), which have different degree of hydrogen bonding with the cobalt phosphates layers (Table 4).

3.2. Magnetic properties

The variable temperature magnetic susceptibility was shown in Fig. 3. The linear behavior of $1/\chi_{(T)}$ above 25 K

Table 4
Hydrogen-bonding geometry for **1**

D···A	D···A (Å)
Ow1···O3	2.78
Ow1···Ow2	2.88
Ow2···N1	3.16
Ow2···O9	2.65
Ow2···OW3	2.57
Ow3···O4	2.71
O10···O4	2.57

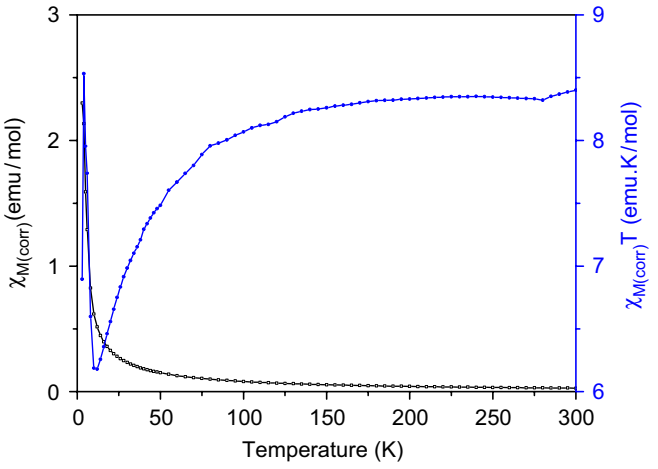

Fig. 3. χ–T and χT–T cuves for **1** under 5000 Oe.

obeys well the Curie–Weiss equation, where $C = 8.6$ emu-K/mol and $\theta = -6.5$ K. The negative value of the Weiss constant indicates antiferromagnetic near-neighbor super-exchange between the Co ions. The effective magnetic moment per cobalt atom calculated from the Curie constant is 4.8 μB, which corresponds to the experimentally observed moment for high-spin Co(= 2 II) ions.

3.3. Thermogravimetric analyses

Thermogravimetric decomposition of **1** was shown in Fig. 4. The first stage, a sharp weight loss from 30 to 250 °C, was ascribed to the removal of tunnel water. The amount of 14.0% was consistent with four water molecules per formula. Three channels water molecules were found in single crystal study. The extra water is probably from the adsorption of water moisture because of the powder sample. The continued behavior was complex. After two continuous weight loss steps from 250 to 465 °C, a regaining weight was observed from ~465 to ~550 °C followed by a weight loss from 550 to a constant weight loss of 32.0% at about 900 °C. The weight loss from 250 to 465 °C mainly is the removal of organic pillar ligands. The reason for weight gain was not clear to us at this moment. However, the combined weight losses can be well ascribed to the removal of organic pillar ligands and water from condensation of POH and bridging hydroxyl groups to

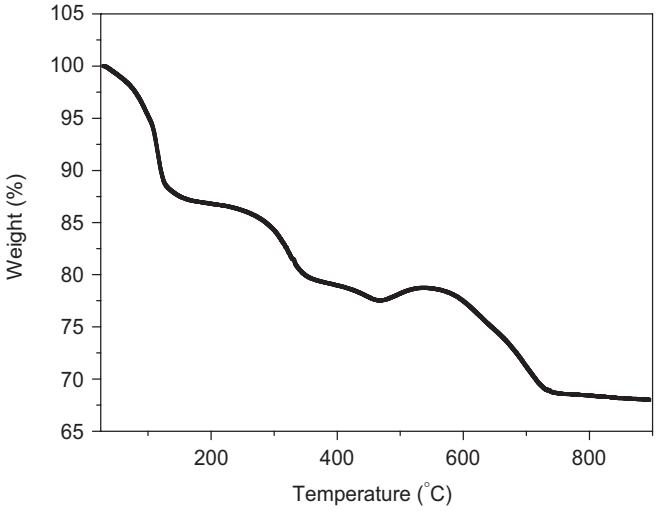

Fig. 4. Thermogravimetric curve of **1**.

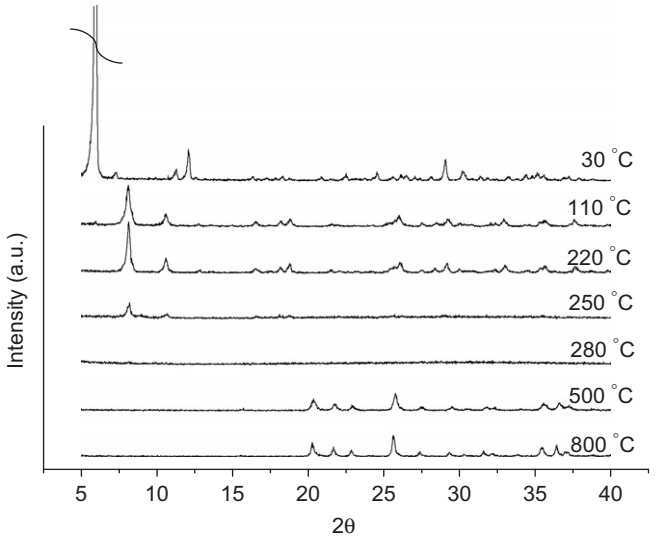

Fig. 5. Variable-temperature in situ XRD patterns of **1**.

formed $Co_3(PO_4)_2$ (theoretical, 31.9%). The phase of residue $Co_3(PO_4)_2$ was checked by XRD.

3.4. Temperature-dependent powder X-ray studies

To understand the structural evolution of compounds **1** at various temperatures, temperature-dependent in situ XRD data were acquired between 30 and 800 °C, Fig. 5. The pattern at 30 °C was consistent well with the pattern simulated from the coordinates of the single-crystal study of **1**. At 110 °C, right after the removal of 2/3 of the tunnel water, the basal spacing of **1** is absent with the formation of new and shorter basal peaks. Furthermore, peaks originated from the layers were shifted. These evidences indicated that the layer crystallinity is still retained. The basal diffraction peak change from 14.3 to 10.9 Å indicating the interlayered spacing shortened seriously on the loss of tunnel water. At 220 °C the situation is similar to that at

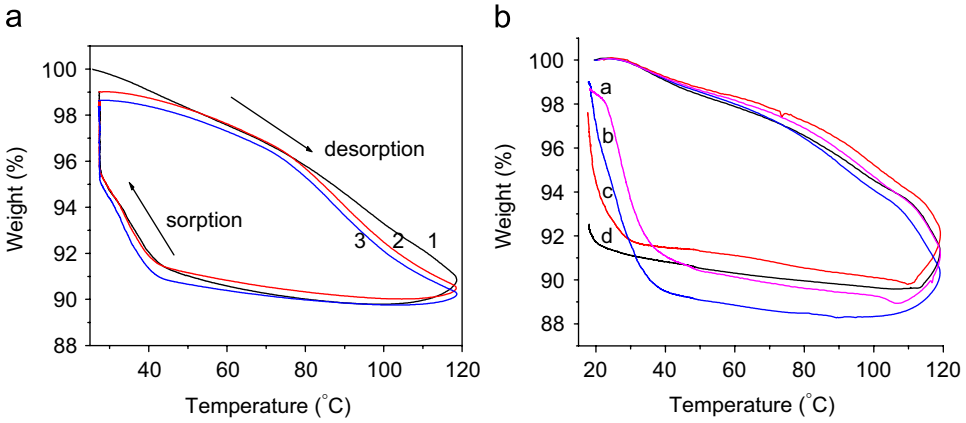

Fig. 6. (a) Three repeated cycles of water desorption/sorption. (b) Organic molecular (a: methanol, b: hexane, c: ether, d: acetone) sorption after partial channel water of **1** is removed.

110 °C. At 250 °C the crystal structure started to break down and at 280 °C it became amorphous. Finally, at 500 °C so as 800 °C the XRD patterns are characteristic peaks of $Co_3(PO_4)_2$ (JCPDS 13-0503).

3.5. Sorption properties

In order to confirm the structural integrity of the dehydrated sample of **1**, sorption experiments were carried out on a thermogravimetric apparatus fitted with a scrubber filled with adsorbate liquids, as described in Section 2. In the water sorption experiments, the sample was first heated to about 120 °C in a flow of dried N_2 gas to remove 2/3 of the water in the tunnels of **1**. Afterwards, the sample was cooled to room temperature and the purged gas is switched to a humidified N_2 gas. These combined heating and cooling steps provide a desorption–sorption cycle for **1**. The reversible dehydration and rehydration processes were evidenced by the losing and regaining weight of the sample. The 90% water molecules were recovered back in the structure. Three repeated cycles of water sorption/desorption have been done and the results are shown in Fig. 6a. In the sorption part of these curves, the appreciable adsorption of water starts from about 40 °C. This is probably because the weak hydrogen bonds between the water molecules and the cobalt phosphate layer take effect at this low temperature. After these experiments, the XRD of the sample showed that crystallinity was unvaried. In a separated run, the sample was heated to 200 °C, the recovery of structure after the contact of water vapor was still observed. Furthermore, similar sorption experiments were carried out for solvent such as acetone, ether, methanol, and hexane. The desorption–sorption curves were shown in Fig. 6b. It demonstrates that **1** can also adsorb organic molecules (10.7% for hexane, 9.7% for methanol, 7.8% for ether, and 2.7% for acetone) with a linear geometry. However, for a sample heated to 200 °C, it did not show any adsorption of organic solvents. This implies that some channel water molecules may play a wedge function to control the up and down positions of the organic bis-N-donor ligands. It is probably because the ligands used in this study are not rigid. Accessible porosity generated by the pillaring effect of organic ligands needs also to be supported by small molecules via the assistance of hydrogen bonding between them and cobalt phosphate layers. It is further suggested that the wedge function may be provided exclusively by the water molecules that support an accessible channel for the further adsorption.

4. Conclusions

A hydrothermal reaction of bis-N-donor ligands, metal salts, and phosphoric acids affords a pillared layer structure with microporous channels filled with water molecules. The water molecules play a wedge function to control the up and down positions for the organic bis-N-donor ligands, which are evidenced from the adsorption–desorption behavior of water molecules and organic molecules.

Acknowledgment

We thank the National Science Council of the Republic of China for supporting this work.

Appendix A. Supplementary materials

Supplementary data associated with this article can be found in the online version at doi:10.1016/j.jssc.2007.03.015.

References

[1] G. Huan, A.J. Jacobson, J.W. Johnson, E.W. Corcoran, Chem. Mater. 2 (1990) 91.
[2] J.W. Johnson, J.F. Brody, R.M. Alexander, Chem. Mater. 2 (1990) 198.

[3] A.J. Jacobson, J.W. Johnson, J.F. Brody, J.C. Scanlon, J.T. Lewandowski, Inorg. Chem. 24 (1985) 1782.
[4] J.W. Johnson, A.J. Jacobson, W.M. Butler, S.E. Rosenthal, J.F. Brody, J.T. Lewandowski, J. Am. Chem. Soc. 111 (1989) 381.
[5] D. Grohol, A. Clearfield, J. Am. Chem. Soc. 119 (1997) 9301.
[6] A. Subbiah, D. Pyle, A. Rowland, J. Huang, R.A. Narayanan, P. Thiyagarajan, J. Zon, A. Clearfield, J. Am. Chem. Soc. 127 (2005) 10826.
[7] F. Fredoueil, D. Massiot, P. Janvier, F. Gingl, B.-D. Martine, M. Evain, A. Clearfield, B. Bujol, Inorg. Chem. 38 (1999) 1831.
[8] Y.-C. Liao, Y.-C. Jiang, S.-L. Wang, J. Am. Chem. Soc. 127 (2005) 12794.
[9] Y.-C. Liao, C.-H. Lin, S.-L. Wang, J. Am. Chem. Soc. 127 (2005) 9986.
[10] Y.-C. Yang, L.-I. Hung, S.-L. Wang, Chem. Mater. 17 (2005) 2833.
[11] A. Clearfield, Z. Wang, J. Chem. Soc. Dalton Trans. (2002) 2937.
[12] P. Yin, S. Gao, L.-M. Zheng, Z. Wang, X.-Q. Xin, Chem. Commun. (2003) 1076.
[13] F. Odobel, D. Massiot, B.S. Harrison, K.S. Schanze, Langmuir 19 (2003) 30.
[14] F. Odobel, B. Bujoli, D. Massiot, Chem. Mater. 13 (2001) 163.
[15] E.V. Bakhmutova, X.D. Ouyang, G. Medvedeve, A. Clearfield, Inorg. Chem. 42 (2003) 7046.
[16] C.-H. Huang, L.-H. Huang, K.-H. Lii, Inorg. Chem. 40 (2001) 2625.
[17] L.-H. Huang, H.-M. Kao, K.-H. Lii, Inorg. Chem. 41 (2002) 2936.
[18] L.-I. Hung, S.-L. Wang, H.-M. Kao, K.-H. Lii, Inorg. Chem. 41 (2002) 3929.
[19] C.-M. Wang, K.-H. Lii, J. Solid State Chem. 172 (2003) 194.
[20] K.-H. Lii, Y.-F. Huang, Inorg. Chem. 38 (1999) 1348.
[21] C.-Y. Chen, F.-R. Lo, H.-M. Kao, K.-H. Lii, Chem. Commun. (2000) 1061.
[22] C.-Y. Chen, K.-H. Lii, J.J. Allan, J. Solid State Chem. 172 (2003) 252.
[23] W.-K. Chang, R.-K. Chiang, Y.-C. Jiang, S.-L. Wang, S.-F. Lee, K.-H. Lii, Inorg. Chem. 43 (2004) 2564.
[24] N. Hamanaka, H. Imoto, Inorg. Chem. 37 (1998) 5844.
[25] G.M. Sheldrick, SADABS, Siemens Analytical X-ray Instrument Division, Madison, WI, 1995.
[26] I.D. Brown, D. Altermatt, Acta Crystallogr. B 41 (1985) 244.
[27] G.M. Sheldrick, SHELXTL Programs, Version 5.1; Brucker AXS, 1998.